Experimental demonstration of an entanglement swapping operation and improved control in NMR quantum-information processing

N. Boulant,[1] K. Edmonds,[2,*] J. Yang,[2,†] M. A. Pravia,[1,‡] and D. G. Cory[1,§]
[1]*Department of Nuclear Engineering, MIT, Cambridge, Massachusetts 02139, USA*
[2]*Center for Materials Science and Engineering, MIT, Cambridge, Massachusetts 02139, USA*
(Received 13 May 2003; published 11 September 2003)

We demonstrate the implementation of an entanglement swapping operation on a four-qubit liquid-state nuclear-magnetic-resonance (NMR) quantum-information processor. We use this experiment as a benchmark to illustrate the progress made in the field of quantum control using strongly modulating pulses and a correction scheme for removing distortions introduced by the nonlinearities in the transmitter and probe circuits. The advances include compensating for incoherent errors caused by the spatial variation of the system Hamiltonian in the NMR sample. The goal of these control sequences is to cause the collapse of the Kraus operator-sum representation of the superoperator into one unitary operator so that the ensemble appears to evolve as one coherent whole.

DOI: 10.1103/PhysRevA.68.032305 PACS number(s): 03.67.Mn

I. INTRODUCTION

Nuclear magnetic resonance (NMR) provides a useful test bed to explore the physical implementations of quantum-information processing (QIP) [1]. Experimental implementations in liquid state have aimed so far at developing coherent control techniques [2], testing quantum algorithms [3–10], performing quantum simulations [11], and exploring open quantum system dynamics (e.g., quantum error correction (QEC) [12–16] and methods to better characterizing decoherence phenomena [17–19]).

We report in this paper on an entanglement swapping operation [20] to illustrate the improvement in quantum control recently gained over spatially incoherent and systematic errors. Counteracting incoherence effects is of fundamental importance for ensemble quantum computing or expectation value quantum computer (EVQC) [21] where the final answer of the computation is given through expectation value measurements and therefore involves a large number of copies of the same quantum system. The power of EVQC would fail if the individual quantum systems did not undergo the desired transformation over some control sequence. It is worth adding that the study presented here while for the spatially incoherence problems seen in liquid-state NMR can also be applied to temporal incoherence where repeated measurements are required to record an expectation value, and the correlation time of the incoherence is long with respect to an individual measurement but short compared to the total expectation value measurement. We first provide a review of the techniques used for the coherent control of nuclear spins including the design of strongly modulating pulses that allow one to implement high fidelity single-qubit gates [2], the modifications necessary to compensate for incoherent errors [22] and a feedback procedure that corrects for systematic radio frequency pulse errors. We then report the experimental results of the entanglement swapping operation. The operation consists of initializing a four-qubit system to a product of pseudosinglet states and performing a measurement in the Bell basis on two qubits shared by the two pairs. This measurement results in the collapse of an initially unentangled qubit subsystem into an incoherent sum of the four Bell states.

II. DESIGN OF SELECTIVE RADIO FREQUENCY PULSES

Weak radio frequency (rf) pulses are usually employed to selectively address chemically shifted spins, where in a small flip angle approximation [23], the profile of the excited magnetization can be approximated as the Fourier transform of the pulse shape. High selectivity therefore requires long times so that the excitation bandwidth is narrow. For QIP, this method suffers the following drawback that the long times required to selectively address spins permits significant decoherence, and all spins continue to evolve under the internal Hamiltonian. For QIP, schemes are required that directly address the propagator rather than finding a gate that can only be applied correctly on a limited set of input states (as is the case commonly encountered in spectroscopy).

A. Internal and external Hamiltonians

To fully explain the complexity of coherently controlling a spatially distributed ensemble, we explicitly introduce the known spatial dependence into the Hamiltonian. Although the spatial functions are straightforward to measure, our goal is to develop control schemes that are independent of the specific spectral variations provided they are within some bounds. It is important to realize that the spatial inhomogeneity introduced into the Hamiltonian is time-independent. The sample is a liquid and the molecular diffusion can play a role [24], but the length scale of the changing Hamiltonian is much longer than the mean molecular displacement on the time scale of the measurement.

*Present address: Department of Chemistry, University of Chicago, Chicago, IL 60637, USA.
†Present address: Departments of Materials Science and Electrical Engineering, UC Berkeley, Berkeley, CA 94720, USA.
‡Present address: Department of Computer Science, University of Puerto Rico, Rio Piedras, PR 00931.
§Corresponding author. Email address: dcory@mit.edu

The internal Hamiltonian of the liquid-state NMR system is

$$H_{int}=\sum_i \Omega_i(\vec{r})I_z^i+2\pi\sum_{i\neq j} J_{ij}\vec{I}^i\cdot\vec{I}^j,$$

where Ω_i is the chemical shift of the ith spin with the spatial location $\vec{r}$ that varies because of the dependence of the external $B_0(\vec{r})$ field, J_{ij} is the scalar coupling constant between spins i and j, and I^i is the spin angular momentum of the ith spin. The scalar coupling constant is spatially independent since it is a through bond interaction that is not mediated by external fields. The external Hamiltonian is

$$H_{ext}=\omega_1(\vec{r},t)\left[\sum_i I_x^i\cos(\Omega t+\phi)+I_y^i\sin(\Omega t+\phi)\right],$$

where ω_1 is the rf power, Ω is the transmitter angular frequency of the radio frequency pulse, t is the time, and ϕ is the initial phase. The dependence of H_{int} on $\vec{r}$ reflects the imperfect homogeneity of the large B_0 external magnetic field while for H_{ext} it reflects the rf inhomogeneity induced by the small excitation/detection coil. We will explore the effect in the reference frame of the rf field so that the spatial variation of ϕ is suppressed. Our goal is to obtain a temporal modulation sequence $H_{tot}(t)$ such that over a specific interval the desired unitary operator $U_{desired}$ is precisely implemented. This is an inverse problem with no known general solution, but the forward problem is quite straightforward. We demonstrate this first for the case without incoherence.

If ω_1, ω, and ϕ are time-independent, then one can move into a rotating frame [25] where the new total effective Hamiltonian (far now with the incoherence suppressed) is

$$\begin{aligned}H_{eff}&=\tilde{H}_{int}+\tilde{H}_{ext}-\Omega\sum_i I_z^i\\&=U_zH_{int}U_z^\dagger+U_zH_{ext}U_z^\dagger-\Omega\sum_i I_z^i\\&=\sum_i(\Omega_i-\Omega)I_z^i+2\pi\sum_{i\neq j}J_{ij}\vec{I}^i\cdot\vec{I}^j\\&\quad+\omega_1\left[\sum_i I_x^i\cos(\phi)+I_y^i\sin(\phi)\right],\end{aligned}$$

where $U_z=\exp[i\Sigma_i I_z^i\Omega t]$ is the frame transformation. As a result, the Hamiltonian in this new frame is time-independent so that the Liouville Von-Neumann equation of motion can be solved exactly

$$\begin{aligned}\tilde{\rho}(t)&=e^{-iH_{eff}t}\tilde{\rho}(0)e^{iH_{eff}t}\\&=e^{-iH_{eff}t}\rho(0)e^{iH_{eff}t},\end{aligned}$$

where ρ denotes the density matrix of the system. To go from the first line to the second one, we note that the two frames coincide at time $t=0$. Obtaining $\tilde{\rho}(t)$ then enables one to obtain $\rho(t)$ by going back to the original frame $\rho(t)=U_z^\dagger\tilde{\rho}(t)U_z$. The net propagator of the evolution of the spin system, for a constant RF power in the rotating frame, can therefore be written as $U=U_z^\dagger(\Omega,t)U_{eff}(\omega_1,\phi,\Omega,t)$, where U_{eff} is the unitary transform corresponding to the evolution only in the rotating frame.

B. Numerical procedure

Since finding a control sequence of arbitrary shape is computationally intractable we attack the simpler problem of piecewise constant Hamitonians and show that there are useful solutions of this form. As was shown in the preceding section, the evolution of the spin system under a pulse of constant parameters can be solved analytically for a given location in the sample. Since the Hamiltonian is time-independent in the rotating frame the equation of motion can be directly integrated without any need of discretization. We note that the resources needed to compute that evolution grow exponentially with the number of qubits but do not increase with the duration of the pulse. In addition, it is easy to see that a single-constant rf power pulse is not sufficient to obtain a selective rotation on a system whose number of spins is larger than 1 because of the internal Hamiltonian and the collective nature of the external Hamiltonian. Our control sequence is a cascade of constant rf pulses, each depending on the four experimental parameters mentioned above, such that the overall operation $U_{net}=\Pi_{k=1}U_z^\dagger(\Omega_k,t_k)U_{eff}(\omega_{(1,k)},\Omega_k,\phi_k,t_k)$ closely approaches the desired unitary operation U_{des}. As a result, this procedure consists of searching for a set of experimental parameters that minimizes $1-|\mathrm{Tr}(U_{des}U_{net}^\dagger(\omega_{(1,k)},\Omega_k,t_k,\phi_k))/N|$, where N is the size of the Hilbert space.

The search respects the limitations of our experimental apparatus through a penalty function on the power, the transmitter frequency and the time (to reduce decoherence effects). The search method is the Nelder-Mead algorithm provided by MATLAB. The algorithm searches for a set of experimental parameters for each square pulse until the fidelity exceeds a threshold, the number of square pulses being increased until the requirement is met. For the three(four)-qubit system of alanine (crotonic acid) in a 300-MHz magnet, the algorithm returns of the order of 0.9995 (0.995) simulated fidelity pulses whose durations are around 200 μs (400 μs). The achievable fidelity strongly depends on the external magnetic field and on the rf power available, which is described in more detail in Ref. [22].

Figure 1 is an example of a strongly modulating pulse designed to perform a selective $\pi/2$ rotation about the x axis on the spins 1 and 2 of alanine (a three-qubit system). The discontinuities indicate the beginning of a new square pulse.

III. COMPENSATION FOR INCOHERENT ERRORS

Due to the spatial extent of the NMR sample, different spins at different locations in the sample see different rf powers and have slightly different chemical shifts. Denoting by $U(\vec{r})$ the unitary operation of the spin system at the location $\vec{r}$, the evolution of the density matrix of the entire sample can be written as an incoherent sum of unitary operations, yielding a potentially nonunitary operation $\rho(t)$

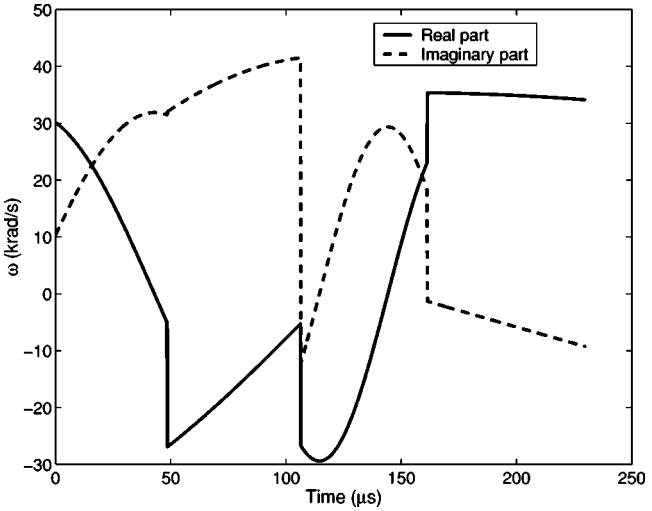

FIG. 1. Strongly modulating pulse for a three-qubit system [$\pi/2$ pulse on spins 1 and 2 of alanine (0.9992 fidelity)]. The ordinate axis represents the power while the horizontal one corresponds to the time.

$=\int U(\vec{r})\rho(0)U^{\dagger}(\vec{r})d\vec{r}$, where we assume a constant density of spins in the sample. The incoherence arising from variations of the chemical shifts and RF power, the evolution of the system can equally be expressed by $\rho(t)=\int p(\omega,\Omega)U(\omega,\Omega)\rho(0)U^{\dagger}(\omega,\Omega)d\omega d\Omega$. This can be viewed as an operator-sum representation of the superoperator [26] where the trace preserving condition in this case simply is $\int p(\omega,\Omega)d\omega d\Omega=1$ so that $p(\omega_i,\Omega_i)$ is the fraction of spins (or probability) that sees a given power ω_i and chemical shift Ω_i. For our experimental setup the variation in resonance frequency is small and simulations in Ref. [2] showed that the fidelity of the pulses varied very little with small variations of chemical shifts. To confirm a close unitary behavior over the sample due to the chemical shifts spread, we simulated our pulses for different sets of chemical shifts (range of ± 5 Hz which is far larger than a typical linewidth in liquid-state NMR), computed the corresponding superoperator, and extracted the Kraus operators. We obtained an operator sum with only two Kraus operators where the norm of the first one was 10^6 times larger than the norm of the second one. This results from the high power of the pulses compared to such small frequency variations. For the remainder of the paper, we will therefore ignore this small effect and focus on the stronger source of incoherence, i.e., rf inhomogeneity. The probability distribution $p(\omega_i,\Omega_i)$ can therefore be replaced to a very good approximation by $p(\omega_i)$. This probability distribution $p(\omega_i)$, that reflects the rf inhomogeneity profile, can be measured using well-known experiments [27]. Once this rf inhomogeneity profile is measured, this information can be incorporated in the design of the selective pulses, by modifying the fidelity metric to include the rf inhomogeneity:

$$F=\sum_{i=1}|\mathrm{Tr}(\sqrt{p(\omega_i)}U(\omega_i)U_{des}^{\dagger})/N|^2.$$

In other words, the algorithm does not search for a sufficiently good local minimum but tries to find a plateau region where the fidelity is robust against small variations in power. The costs of this procedure are the longer times it takes to find a solution, a larger number of periods, and an increase in the duration of the pulses.

An alternate form to the operator-sum representation of the superoperator is the Liouville representation [28], i.e.,

$$S=\sum_{i=1}p(\omega_i)\overline{U}_i\otimes U_i,$$

where S is the superoperator in the Zeeman basis [28] and $\overline{U}$ denotes the complex conjugate of U. This form of the superoperator can be applied to the density matrix once it has been columnized by stacking its columns on top of each other. S being a convex sum of unitary operators is generally a nonunitary operator so that its eigenvalues lie inside the unit circle. In Fig. 2, we plot in the complex plane the eigenvalues of two calculated superoperators obtained with and without incorporating RF inhomogeneity in the design of the pulses.

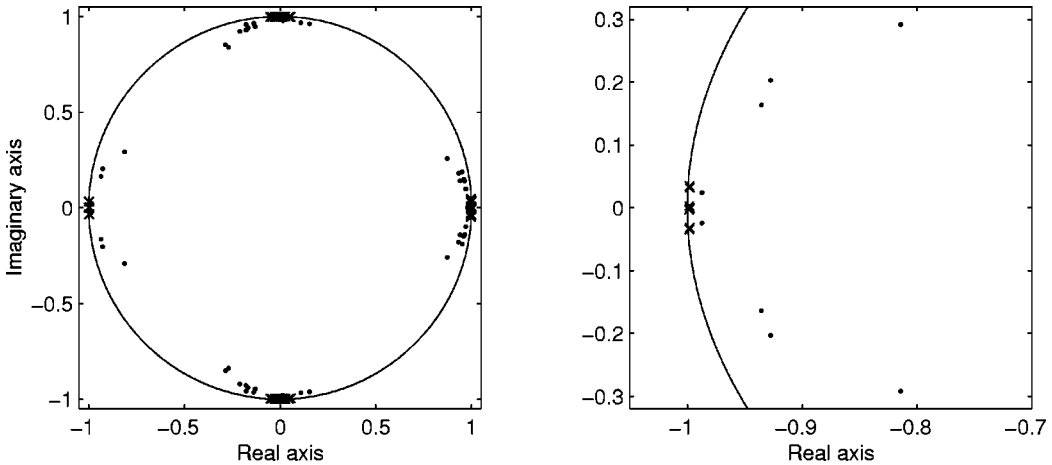

FIG. 2. Eigenvalue spectrum of the superoperators corresponding to a compensated and noncompensated pulse (for a three-qubit system). The dots correspond to the noncompensated scenario while the crosses correspond to the compensated pulse. The crosses lie quite close to the unit circle while the dots are spread inside.

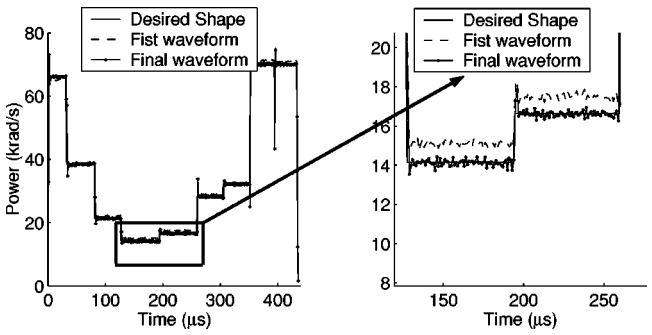

FIG. 3. Distorted and corrected rf amplitude. The solid line represents the desired shape, while the dashed and dot-dashed lines correspond to the initial measured waveform and the final one (after two iterations of the feedback code), respectively. The high-frequency transients present at the transitions between periods have little effect on the overall performance of the gates.

The eigenvalues of the noncompensated pulse are inside the unit circle while the ones of the compensated one are close to the unit circle. As a rough indication, the minimum modulus of the eigenvalues for the noncompensated pulse is 0.865, while the smallest one for the robust pulse is 0.998. In addition, we extracted the Kraus operators from the two superoperators. In both cases, we obtained three Kraus operators. For the noncompensated pulse, the norm of the second and third Kraus operators were equal to 4% and 0.06% of the first one, respectively, while the numbers were 0.13% and 0.01% for the compensated one. Within this degree of precision (around 0.1%), the entire superoperator can be approximated by one unitary operator. By including in the design of the pulses the rf inhomogeneity information, the Kraus operator-sum representation has therefore collapsed into one operator very close to being unitary. The improvement is clear and shows a significant approach towards a truly unitary behavior.

IV. CORRECTING FOR rf DISTORTIONS

Although simulations of the pulses demonstrate that the gates are relatively robust against small deviations in some of the control parameters, a substantial loss of fidelity occurs when the rf amplitudes deviate from the prescribed values. The experiment to be discussed in the following section was performed on a 400-MHz Bruker Avance spectrometer. In this spectrometer, a digital waveform generator creates the desired shape at low power. The signal is then amplified and routed to the probe that is a tuned resonant circuit at the carbon resonance frequency ($\sim$100 MHz). The system transfer function is frequency dependent and to some extent power dependent (due to small nonlinearities in the power amplifier). Since we are interested in the rf modulation that the spins see, the easiest approach is to directly measure this in the NMR probe and then correct the waveform in an iterative step. We have measured that the maximum deviation from the ideal power is about 125 Hz out of 3 KHz (Fig. 3), while the mean phase deviations are comparatively small, about 0.7 deg.

Based on the simulation in Ref. [2], we can expect that the phase errors cause negligible loss in fidelity. However, the amplitude errors cause the rf nutation rate in each period to vary by up to 4% for typical crotonic acid (four-qubit-system made of four labeled ^{13}C nuclei) pulses, resulting in a significant drop in fidelity. Simulations of crotonic gates with the rf power set to 4% smaller than the ideal power have fidelities about 0.01 smaller than the fidelities of the ideal transformations.

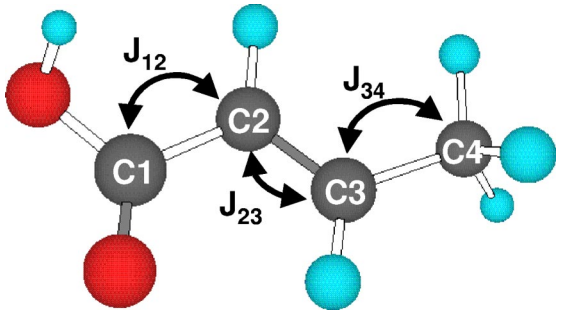

FIG. 4. Molecule of crotonic acid. The chemical shifts are $\nu_1 = 6878.9$ Hz, $\nu_2 = 1882.6$ Hz, $\nu_3 = 4410.1$ Hz, and $\nu_4 = -8604.9$ Hz, while the J coupling constants are $J_{12} = 72.4$ Hz, $J_{13} = 1.4$ Hz, $J_{14} = 7.2$ Hz, $J_{23} = 69.6$ Hz, $J_{24} = 1.6$ Hz, and $J_{34} = 41.5$ Hz.

To correct the amplitude and phase errors, we use an iterative feedback procedure to determine the low power RF waveforms that, when sent through the transmitter chain, will create a rf shape close to the intended shape. The rf measurement uses the hydrogen coil as a spy pickup antenna to observe the final carbon rf wave transmitted to the sample. The hydrogen resonant circuit is tuned to 400 MHz, and as a result it attenuates the 100-MHz carbon signals by about 30 dB. Since the proton circuit does not have any resonance near the carbon frequency, its response is nearly flat over a 1-MHz band around the carbon resonance frequency. Therefore we can use the proton channel as a nonresonant inductive pickup coil for the carbon field at the sample.

V. EXPERIMENTAL BENCHMARK: THE ENTANGLEMENT SWAPPING EXPERIMENT

We report in this section the implementation of an entanglement swapping experiment to illustrate the gain in control achieved, given the compensations for the errors presented above. In addition, this experiment shows the manipulation of entanglement through measurements. It was demonstrated in Ref. [20] that entanglement can be teleported from one pair of photons to another when the quadruple contains two singlet states among disjoint pairs, an effect that has been argued to show that quantum correlations are as nonlocal as the quantum states themselves [29].

A. The experiment

This demonstration was carried out on a liquid-state NMR quantum-information processor, using the four ^{13}C labeled nuclei in a sample of crotonic acid (see Fig. 4) as the qubits and a Bruker Avance 400-MHz spectrometer for the control and acquisition. The experiment consisted of initializing the

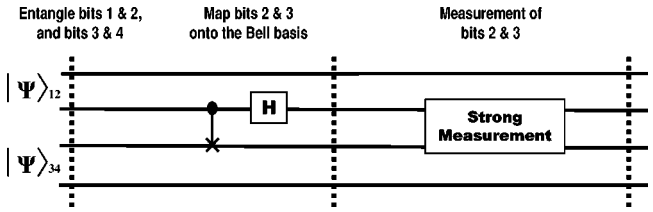

FIG. 5. Logical network for the entanglement swapping experiment.

system to a full four-spin pseudopure state made of two pairs of singlet states and then performing on two of these qubits a Bell measurement, each one belonging to a different pair (an NMR version of Ref. [20]) (see Fig. 5). The protons were decoupled only during acquisition to avoid nuclear overhauser enhancement [25]. During the gate sequence, the proton-carbon couplings were refocused using π pulses on the carbon channel.

Since liquid-state NMR deals with a highly mixed ensemble of spin systems, we stress that the use of pseudopure states allows a macroscopic description of the same unitary dynamics to which the microscopic systems are subjected [30,31]. The experiment described here does not depend on the entanglement within the individual molecules.

The traceless part of the density matrix was prepared in a state isomorphic to

$$|\Psi\rangle_{1234}=\tfrac{1}{2}(|01\rangle_{12}-|10\rangle_{12})\otimes(|01\rangle_{34}-|10\rangle_{34}),$$

which can be rewritten as

$$|\Psi\rangle_{1234}=\tfrac{1}{2}(|\Psi^+\rangle_{14}|\Psi^+\rangle_{23}+|\Psi^-\rangle_{14}|\Psi^-\rangle_{23}+|\Phi^+\rangle_{14}|\Phi^+\rangle_{23}+|\Phi^-\rangle_{14}|\Phi^-\rangle_{23}),$$

where $\Psi^{\pm}$ and $\Phi^{\pm}$ correspond to the four Bell states. Performing a measurement on qubits 2 and 3 in the Bell basis projects qubits 1 and 4 onto one of the four Bell states with probabilities equal to 1/4. The entanglement thereby is transferred between two pairs of spins. This experiment includes the first four-qubit initialization to a full spatial pseudopure state. Because all the elements of the density matrix are not directly observable, state tomography [32] was performed with a total of 18 separate measurements. The readout pulses are the order of 400 μs and do not introduce significant decoherence. To measure the accuracy with which the experiment was performed and to compare it with Ref. [33], we calculated the correlation (or sometimes called projection)

$$C=\frac{\mathrm{Tr}(\rho_{expt}\rho_{theory})}{\sqrt{\mathrm{Tr}(\rho_{expt}\rho_{expt})\mathrm{Tr}(\rho_{theory}\rho_{theory})}}.$$

If ρ_{expt} and ρ_{theory} are viewed as vectors, then this metric is the directional cosine between the experimental and desired density matrices. The sequence used to initialize the spin system to the pseudopure state was derived from Ref. [35]. We stress that, once the NMR spectrometer had been calibrated and the strongly modulating pulses programmed, no further adjustments of any kind were required (or made) during the course of the measurements that made up this study. The correlation of the initialized density matrix is 0.929 (the real part of the density matrix is plotted in Fig. 6), while the correlation of the final density matrix, i.e., after the Bell measurement, is 0.90 (see Fig. 7).

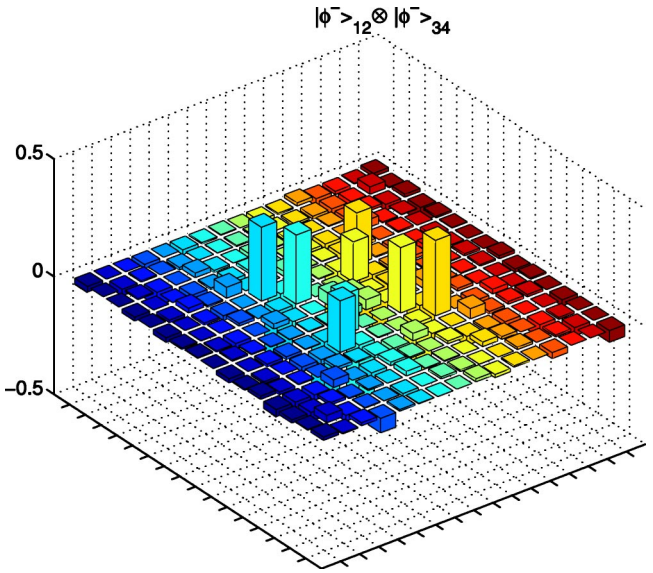

FIG. 6. Real part of the initial density matrix (product of singlet states). The rows and columns represent the standard computational basis in binary order, with $\langle 0000|$ starting from the leftmost column and $\langle 1111|$ being the rightmost column.

The experiment consisted of 65 pulses with a total duration of 121 ms. This may be compared to the experiment in Ref. [33], which used 44 pulses, lasted 75 ms, and yielded a final correlation of 0.79. This experiment with a correlation of 0.90, confirms the increased level of control. In addition,

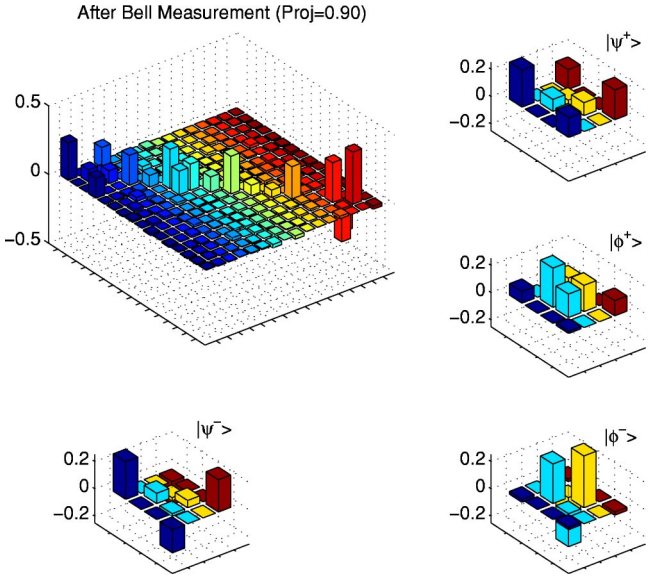

FIG. 7. Bell states. For the sake of convenience, the labels of the spins have been switched so that the pattern characteristic of the Bell states is more clear. Now the ket $|0000\rangle$ should be interpreted as $|0\rangle_2\otimes|0\rangle_3\otimes|0\rangle_1\otimes|0\rangle_4$. One can see that the measurement results in an equal mixture of the four Bell states. For clarity, we zoomed on the submatrices along the diagonal to show the Bell states more clearly ($|\psi^{\pm}\rangle=(1/\sqrt{2})(|00\rangle\pm|11\rangle)$, $|\phi^{\pm}\rangle=(1/\sqrt{2})(|01\rangle\pm|10\rangle)$).

simulations of the full spin system (including the protons) without decoherent effects using the new design of the pulses yielded a correlation of 0.935 for the initial pseudopure state and 0.87 using the previous design, providing further evidence of improved control. The sample has a dephasing time T_2 of the order of 600 ms, and we assume that most of the differences between the measurements and simulation arise from decoherence. Because different elements in the density matrix decay with different rates, decoherence not only attenuates the magnitude of the density matrix $\mathrm{Tr}(\rho^2)$ but it also rotates it so that the correlation between the two density matrices is reduced.

B. Measurement in the Bell basis

In this study, measurement in the Bell basis is replaced with dephasing, which is more conveniently carried out in the Zeeman basis (see Ref. [34] for a detailed description). The mapping from the Bell to the Zeeman basis can be performed by applying a controlled NOT gate on qubits 2 and 3 followed by an Hadamard on only qubit 2. After the dephasing in the Zeeman basis, the inverse mapping should be applied to return the system to the original basis. However, in the network shown in Fig. 5 this inverse mapping was not included for the sake of clarity, i.e., to exhibit the structure of the four Bell states shown in Fig. 7. The measurement in the computational basis destroys phase coherences between the two spins of interest. Experimentally this was accomplished using the nonunitary dynamics of magnetic-field gradients integrated over the spatially distributed sample [35]. Because a gradient evolution superimposes a linear phase ramp on the chemical shift function of position, the resulting spatial average over the ensemble destroys any phase coherence between the spins. In the simulation to be described, the amount of entanglement transferred to qubits 1 and 4 clearly depends on the selective decoherence of qubits 2 and 3. The input state in this simulation is the measured experimental density matrix $\rho_{singlet}$ given in Fig. 6, on which the simulated unitary operator $U_{Bell\ map}$ which maps the Bell basis to the Zeeman one is applied. The state then goes through a measurement process, represented by the following Kraus operator-sum representation:

$$\rho_{out} = \sum_{k=1}^{5} A_k \rho_{in} A_k^{\dagger},$$

where $A_1 = \sqrt{(1-\alpha^2)}I$, $A_2 = \alpha(|00\rangle\langle 00|)_{23}$, $A_3 = \alpha(|01\rangle\langle 01|)_{23}$, $A_4 = \alpha(|10\rangle\langle 10|)_{23}$, and $A_5 = \alpha(|11\rangle\langle 11|)_{23}$ and where by $(|\psi\rangle\langle\psi|)_{23}$ we mean the projectors in the subspace of qubits 2 and 3 (note that the trace preserving condition is satisfied $\Sigma_{k=1}^{5} A_k^{\dagger} A_k = I$). The value of α is then varied to study the entanglement transfer as a function of the strength of the measurement, $\alpha = 1$ corresponding to a strong measurement and $\alpha = 0$ to no measurement. In Fig. 8, we plot as a function of α the correlation between ρ_{out}, obtained by doing the simulation described above, and ρ_{th} (the maximally entangled theoretical density matrix).

This plot shows the amount of entanglement transferred as a function of the strength of the measurement. The correlation between our measured output density matrix and the theoretical one was 0.90. Figure 8 thereby reveals that we reached a precision of better than 5% ($\alpha > 0.95$) for the implemented selective decoherence.

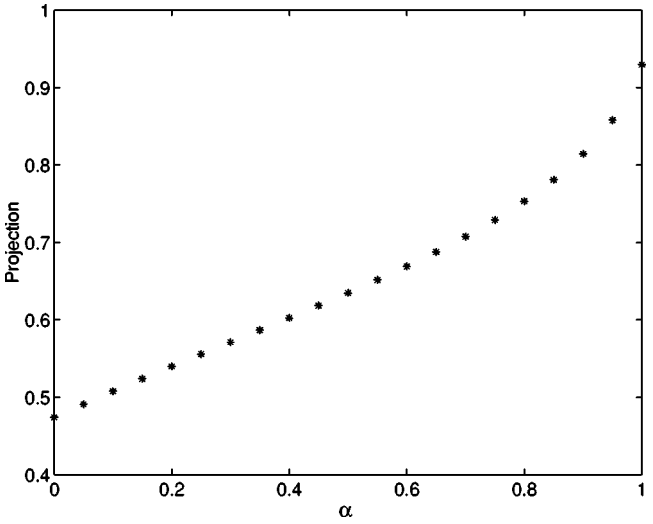

FIG. 8. Entanglement transfer efficiency vs the strength of the measurement. For $\alpha = 1$ the correlation between the simulated ρ_{out} and the theoretical density matrix is equal to 0.93. This value being less than 1 is due to the nonperfect experimental input state and to the coherent errors contained in $U_{Bell\ map}$.

VI. CONCLUSION

We reported in this paper the improvements gained in quantum coherent control when information about the types of time-independent errors is used to design strongly modulating pulses. We reviewed the key ingredients of the design, calibration, and correction of these pulses. Furthermore, we showed that incorporating these features in the design of the pulses allowed to obtain an evolution very close to being unitary for single-qubit gates. We also reported on the implementation of an entanglement swapping experiment to compare its results with the ones in Ref. [33]. We believe this comparison is appropriate as they were both performed on the same four qubit system with only the experiment described here incorporating compensation against incoherent and systematic waveform errors. We reconstructed the density matrices at the key steps and extracted the correlations. These numbers, along with the length of the experiment and the number of pulses compared to the ones for Ref. [33], indicates a net improvement of coherent control. We believe these techniques can be applied for a wide variety of quantum devices where precise coherent control is required.

ACKNOWLEDGMENTS

This work was supported by ARO through Grant Nos. DAAD19-01-1-0519 and DAAD19-01-1-0678, Grant. DARPA MDA972-01-1-0003, and NSF Grant No. EEC0085557. We thank T. F. Havel for valuable discussions.

[1] D.G. Cory, R. Laflamme, E. Knill, L. Viola, T.F. Havel, N. Boulant, G. Boutis, E. Fortunato, S. Lloyd, R. Martinez, C. Negrevergne, M. Pravia, Y. Sharf, G. Teklemariam, Y.S. Weinstein, and W.H. Zurek, Fortschr. Phys. **48**, 875 (2000).
[2] E.M. Fortunato, M.A. Pravia, N. Boulant, G. Teklemariam, T.F. Havel, and D.G. Cory, J. Chem. Phys. **116**, 7599 (2002).
[3] L.M.K. Vandersypen, M. Steffen, G. Breyta, C.S. Yannoni, M.H. Sherwood, and I.L. Chuang, Nature (London) **414**, 883 (2001).
[4] K. Dorai, Arvind, and A. Kumar, Phys. Rev. A **61**, 042306 (2000).
[5] N. Linden, H. Barjat, and R. Freeman, Chem. Phys. Lett. **296**, 61 (1998).
[6] J.A. Jones and M. Mosca, J. Chem. Phys. **109**, 1648 (1998).
[7] I.L. Chuang, L.M.K. Vandersypen, X. Zhou, D.W. Leung, and S. Lloyd, Nature (London) **393**, 143 (1998).
[8] I.L. Chuang, N. Gershenfeld, and M. Kubinec, Phys. Rev. Lett. **80**, 3408 (1998).
[9] J.A. Jones, M. Mosca, and R.H. Hansen, Nature (London) **393**, 344 (1998).
[10] J.A. Jones, Science **280**, 229 (1998).
[11] S. Somaroo, C.-H. Tseng, T.F. Havel, R. Laflamme, and D.G. Cory, Phys. Rev. Lett. **82**, 5381 (1999).
[12] E. Knill, R. Laflamme, R. Martinez, and C. Negrevergne, Phys. Rev. Lett. **86**, 5811 (2001).
[13] L. Viola, E.M. Fortunato, M.A. Pravia, E. Knill, R. Laflamme, and D.G. Cory, Science **293**, 2059 (2001).
[14] E.M. Fortunato, L. Viola, J. Hodges, G. Teklemariam, and D.G. Cory, New J. Phys. **4**, 5.1 (2002).
[15] D.G. Cory, M.D. Price, W. Maas, E. Knill, R. Laflamme, W.H. Zurek, T.F. Havel, and S.S. Somaroo, Phys. Rev. Lett. **81**, 2152 (1998).
[16] N. Boulant, M.A. Pravia, E.M. Fortunato, T.F. Havel, and D.G. Cory, Quantum Information Processing **1**, 135 (2002).
[17] N. Boulant, T.F. Havel, M.A. Pravia, and D.G. Cory, Phys. Rev. A **67**, 042322 (2003).
[18] A.M. Childs, I.L. Chuang, and D.W. Leung, Phys. Rev. A **64**, 012314 (2001).
[19] G. Teklemariam, E.M. Fortunato, C.C. Lopez, J. Emerson, J.P. Paz, T.F. Havel, and D.G. Cory, Phys. Rev. A **67**, 062316 (2003).
[20] J-W. Pan, D. Bouwmeester, H. Weinfurter, and A. Zeilinger, Phys. Rev. Lett. **80**, 3891 (1998).
[21] D.G. Cory, A.F. Fahmy, and T.F. Havel, Proc. Natl. Acad. Sci. U.S.A. **94**, 1634 (1997).
[22] M.A. Pravia, N. Boulant, J. Emerson, E. Fortunato, A. Farid, T.F. Havel, and D.G. Cory (unpublished).
[23] A. Sodickson and D.G. Cory, Prog. Nucl. Magn. Reson. Spectrosc. **33**, 77 (1998).
[24] P.T. Callaghan, *Principles of Nuclear Magnetic Resonance Microscopy* (Oxford University Press, Oxford, 1991).
[25] R.R. Ernst, G. Bodenhausen, and A. Wokaun, *Principles of Nuclear Magnetic Resonance in One and Two Dimensions* (Oxford University Press, Oxford, 1994).
[26] J. Preskill, http://www.theory.caltech.edu/people/preskill/ph229
[27] S. Reich, and A.J. Vega, J. Appl. Phys. **58**, 2759 (1985).
[28] T.F. Havel, J. Math. Phys. **44**, 534 (2003).
[29] A. Cabello, Phys. Rev. A **59**, 113 (1999).
[30] D.G. Cory, A.F. Fahmy, and T.F. Havel, in *Proceedings of PhysComp 96*, edited by T. Toffoli, M. Biafore, and J. Leão (New England Complex Systems Institute, Cambridge, MA, 1996), pp. 87–91.
[31] N.A. Gershenfeld and I.L. Chuang, Science **275**, 350 (1997).
[32] I.L. Chuang, N. Gershenfeld, M. Kubinec, and D. Leung, Proc. R. Soc. London, Ser. A **454**, 447 (1998).
[33] N. Boulant, E.M. Fortunato, M.A. Pravia, G. Teklemariam, D.G. Cory, and T.F. Havel, Phys. Rev. A **65**, 024302 (2002).
[34] G. Teklemariam, E.M. Fortunato, M.A. Pravia, Y. Sharf, T.F. Havel, D.G. Cory, A. Bhattaharyya, and J. Hou, Phys. Rev. A **66**, 012309 (2002).
[35] G. Teklemariam, E.M. Fortunato, M.A. Pravia, T.F. Havel, and D.G. Cory, Phys. Rev. Lett. **86**, 5845 (2001).